Investigation of dynamical heterogeneities in polymer melts

Rupam Borah, Nabi Ahamad and Pallavi Debnath*

Department of Chemistry, Indian Institute of Technology Roorkee, Roorkee 247 667, India

In this paper, dynamical heterogeneities are characterized both at the monomer and centre-of-mass level, in polymer melts well above their glass transition temperature, responsible for anomalous dynamics in these systems. Microscopic analysis of united atom molecular dynamics simulations of unentangled polyethylene melts suggests a molecular mechanism for the observed heterogeneous dynamics based on local density fluctuations about a tagged polymer. These local density fluctuations are related to variations in entropy in a small volume about a polymer in the melt, which result in initial connections of the dynamical heterogeneities to entropy.

Keywords: Dynamics, heterogeneities, microscopic analysis, polymer melts.

THE term 'dynamical heterogeneities' encompasses transient clusters of particles with enhanced or reduced mobility relative to the average in time intervals $t < \tau_{\text{Rouse}}$ (where τ_{Rouse} is the longest intramolecular relaxation time, and defined as the time a molecule requires to diffuse a distance comparable to its own dimension, radius of gyration R_g). These high and low mobility regions fluctuate throughout the sample in time. Many theoretical and experimental studies show that polymer melts and glass-forming liquids display heterogeneous dynamics near glass transition temperature, or under supercooled, or undercooled conditions[1–7]. The possibility of dynamical heterogeneities in these systems, specifically polymer melts well above their glass transition temperature, is rather less reported. In this paper we investigate, characterize dynamical heterogeneities in polymer melts well above their glass transition temperature, and attempt to address the molecular origin of these transient high and low mobility regions in the melt.

Polymer melts display short-time anomalous dynamics in disagreement with conventional single-molecule mean-field theories – namely Rouse and reptation models for dynamics in unentangled and entangled systems respectively[8–11]. This anomalous dynamics includes subdiffusive centre-of-mass (c.m.) dynamics and anomalous segment diffusion, and has been attributed to dynamical heterogeneities in these liquids[12]. Consequently, a theory which defines the relevant variables as momenta and space coordinates of the molecules comprising the low mobility region and projects the fluid dynamics onto these variables – namely the cooperative dynamics generalized Langevin equation (CDGLE) formalism – could correctly predict the observed anomalous dynamics of monomer and c.m. in the complete range of timescale of interest, from the prediffusive to the diffusive regime[12]. But CDGLE approach does not discuss the origin of dynamical heterogeneities.

In spite of considerable experimental and theoretical effort in the past two decades, the origin of dynamic heterogeneities remains an open question for many systems[13,14]. Glotzer and co-workers observed string-like correlated motion in the dynamics of simulated supercooled unentangled polymer melts and related this motion to dynamical heterogeneities[1]. Based on these findings and further work, string model of glass formation[15] is explored to study different aspects of glass formation and dynamical heterogeneities in polymer melts[16]. Still the origin of dynamical heterogeneities is not explained in these studies. We provide useful insights into this question in polymer melts well above glass transition temperature by microscopic analysis of united atom molecular dynamics (UA-MD) simulation trajectories of unentangled polyethylene melts from G. S. Grest and coworkers[17,18] and V. G. Mavrantzas and coworkers[19].

The following section discusses the analysis of heterogeneous dynamics in unentangled polyethylene (PE) melts well above their glass transition temperature. The next following section suggests a molecular mechanism of the observed dynamical heterogeneities, that evolves from the microscopic analysis, relating the rapid switch from slow to fast dynamics of a tagged chain to density fluctuations. Later, we discuss the associated estimation of entropy about the tagged chain. Conclusions are drawn at the end.

Characterization of heterogeneous dynamics

We analyse heterogeneous dynamics in UA-MD simulation trajectories of unentangled polyethylene melts from research groups of G. S. Grest[17,18] and V. G. Mavrantzas[19]. These UA-MD simulation data from the research groups[17–19] mentioned, exhibited excellent agreement with CDGLE theory[12]. The details of the UA-MD simulation data analysed are given in Table 1. G. S. Grest and coworkers[17,18] performed simulations for all N (except C_{100}) under isothermal-isochoric conditions, while V. G.

*For correspondence. (e-mail: pdebhfcy@iitr.ac.in)

Mavrantzas and coworkers[19] performed simulations for $N = 100$ on an *NPT* ensemble over a group of n chains. The characteristic longest timescale, for these unentangled melts is τ_{Rouse}, defined as the time taken by a chain in the melt to diffuse a distance comparable to its own dimension, R_g, and thus written as $\tau_{Rouse} = R_g^2/D$ (where D is the diffusion coefficient), and calculated in Table 1. This timescale is also the characteristic relaxation time of dynamical heterogeneities as shown in Figure 1 *a* and *b* for monomer dynamics. Self-part of the monomer van Hove distribution function $G_s(\Delta r, t)$, represents the probability of monomer displacement Δr in time interval t, which can be shown to be Gaussian if harmonic intramolecular potential is assumed as shown explicitly in the appendix (eq. A15). In a purely diffusive system $G_s(\Delta r, t)$ is expected to be a single mode Gaussian. Figure 1 *a* and *b* show representative radial distributions of monomer displacements sampled at fixed time intervals $t < \tau_{Rouse}$ and $t = \tau_{Rouse}$. These distributions are fitted to a Gaussian distribution (dashed line) in Figure 1 *a*, while the derived equation (eq. A15) is shown in solid line (Figure 1 *a* and *b*). The derived $G_s(\Delta r, t)$ (eq. A15) does not show good agreement with simulation data for $t < \tau_{Rouse}$ (Figure 1 *a*), but provides excellent fit to the simulation data for time intervals $t \geq \tau_{Rouse}$ (Figure 1 *b*). For $t < \tau_{Rouse}$ the distribution of monomer displacements shows a non-Gaussian tail at large displacements due to a fast dynamical process in addition to the slow diffusive process in the polymer melt system. At times $t \approx \tau_{Rouse}$, the distribution becomes Gaussian as dynamical heterogeneities are averaged out and the trajectories follow free diffusion. Similar conclusions from analysis of c.m. dynamics can be found elsewhere[12].

Correlation between chain stretching and fast diffusion

For times $t < \tau_{Rouse}$, the probability distribution for monomer displacement (Figure 1) and c.m. displacements[12] (not shown) exhibit non-Gaussian tail at large displacements, implying a fraction of monomers and c.m.s move farther than the rest, respectively, and are considered to be more mobile. We analyse c.m. displacements at such selected time intervals $t < \tau_{Rouse}$, where maximum deviation of probability distributions for monomer and c.m. displacements from that expected of Gaussian approximation (which holds for purely diffusive motion), is obtained. Evidently at these time intervals maximum heterogeneity in dynamics is exhibited, which implies more fraction of monomers or c.m.s perform very fast motion and pronounced non-Gaussian tail is obtained at larger displacements in the distributions for both c.m. and monomer displacements. The correlation between c.m. displacements and average end-to-end distances for the time interval t that maximizes this contribution due to the fast dynamical process is studied. Figure 2 *a*, *b* and *c* show representatively the results for $C_{16}H_{34}$ at $t = \tau_{Rouse}/2$, $C_{44}H_{90}$ at $t = \tau_{Rouse}/7.6$, and $C_{100}H_{202}$ at $t = \tau_{Rouse}/2.3$, respectively. The different colours represent contour plots of the three-dimensional distribution function. A point with its colour on this contour plot represents the probability that a polymer exhibits c.m. displacement ΔR in time interval t with end-to-end distance R_{ete}, in a scale of 2–11. Hence darker colours represent lesser probability and vice-versa. The melts of short polymer chains (Figure 2 *a* and *b*) distinctly show that the fast dynamical relaxation is correlated with the appearance of persistent stretched configurations comprising high percentage of trans conformations. However, completely stretched configurations are entropically unfavourable (except for very short chains like C_{16} (Figure 2 *a*)), and become less probable

Table 1. Parameters for the UA-MD simulation trajectories[17–19]

System	N	n	T (K)	L (Å)	τ_{Rouse} (ns)
$C_{16}H_{34}$	16	64	323	31.7	0.26
$C_{30}H_{62}$	30	64	400	39.3	0.83
$C_{44}H_{90}$	44	100	400	51.4	2.35
$C_{96}H_{194}$	96	400	448	105.4	15.30
$C_{100}H_{202}$	100	48	450	52.9	18.73

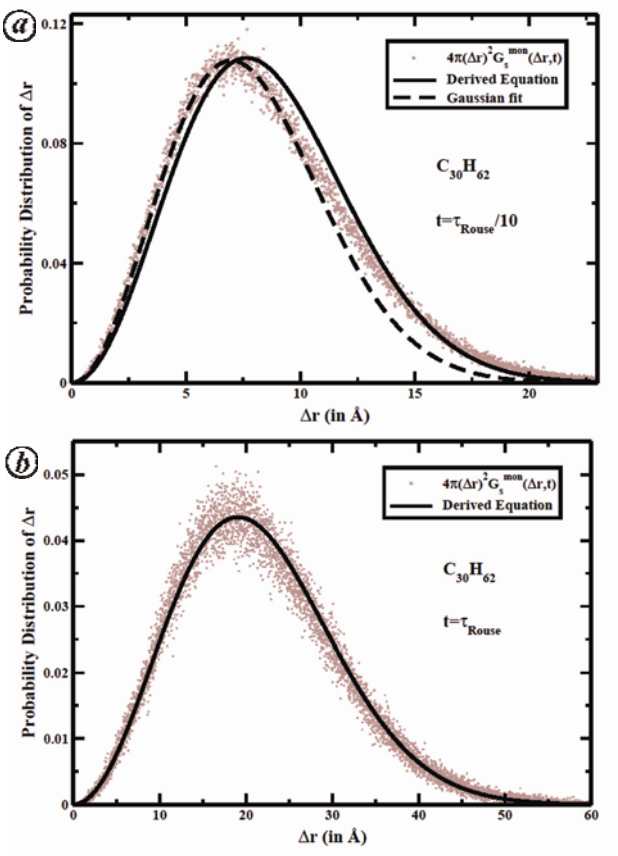

Figure 1. Distribution of monomer displacements for $C_{30}H_{62}$ at fixed time intervals (***a***) $t < \tau_{Rouse}$ and (***b***) $t \cong \tau_{Rouse}$. Unfilled coloured circles: UA-MD simulation data. Dashed line: best fit (single mode Gaussian distribution) to slow dynamics. Solid line: as calculated from eq. (A15) with $\langle(\Delta r)^2\rangle$ input from the simulation.

with increasing polymer length. In fact, for the high molecular weight sample as seen in Figure 2 *c* the appearance of stretched configurations becomes a rare event as they are entropically unfavourable since the difference in entropy of Gaussian chain at non-zero extension from its zero extension value, scales as $\Delta S \propto -N$ (ref. 20).

In Figure 2 *a*–*c*, the polymer molecules in blue regions on the top right corner, exhibit fast dynamics and also maximum heterogeneity in dynamics (as explained above); are subjected to further investigation. The c.m. of these molecules shows transient periods of very small amplitude (slow) motion followed by periods of distinctly large amplitude (fast) motion, which also implies that the molecule trajectory switches from transient low mobility to high mobility regions as explained in the next section (also see Figure 4). Figure 3 *a* and *b* show a representative result from one such study done on a tagged polymer 10 of $C_{100}H_{202}$ melt, where the correlation between the stretching and fast dynamics is explored further at fixed time interval $t = 8.0$ ns where polymer 10 exhibited maximum heterogeneity in dynamics. The c.m. displacement $\Delta R(t)$ in Figure 3 *a* is given by $\Delta R(t) = |\mathbf{R}(t_2) - \mathbf{R}(t_1)|$, where $t_2 - t_1 = t$. Projections of $\Delta\mathbf{R}(t)$ in the direction of end-to-end distance $\mathbf{R}_{ete}$ are averaged over the fixed time interval t as $\Delta\mathbf{R}\cdot\hat{\mathbf{R}}_{ete} = (X_{ete}^2 + Y_{ete}^2 + Z_{ete}^2)^{-1/2}\ (\Delta XX_{ete} + \Delta YY_{ete} + \Delta ZZ_{ete})$. The *x*-, *y*- and *z*-components of $\mathbf{R}_{ete}$ in this expression are averaged over the fixed time interval *t*, while components of $\Delta\mathbf{R}$ are obtained as explained above (for its magnitude $\Delta R(t)$). The magnitude of the c.m. displacement along the direction perpendicular to $\mathbf{R}_{ete}$ is calculated as $|\Delta\mathbf{R}\times\hat{\mathbf{R}}_{ete}| = [(\Delta R)^2 - (\Delta\mathbf{R}\cdot\hat{\mathbf{R}}_{ete})^2]^{1/2}$. The mean square displacements, the projections of $\Delta\mathbf{R}(t)$ along and perpendicular to end-to-end distance, and the end-to-end distance values averaged over fixed time interval *t* are shown in Figure 3 *a* and *b*, where the *x*-axes are the lower bounding step numbers of the instances (sequences) of *t* as it occurs in the UA-MD simulation trajectory. For example, values of '0' and '5' of steps-axis (*x*-axes in Figure 3) represent instances of time interval of $t = 8.0$ ns occurring between (0–80)th and (5–85)th steps respectively (0.1 ns/step, i.e. trajectories were recorded by V. G. Mavrantzas and coworkers[19] after every 0.1 ns). Thus *x*-axes in Figure 3 give the direction of time in the trajectory of the molecule, and the results are shown over the entire trajectory. The *y*-axis values of the curve labelled R_{ete} in Figure 3 *a* are averaged over fixed time interval *t*; for example, the value at steps-axis value = 5 (say) represents end-to-end distance averaged over all the steps from 5th to 85th step of the tagged polymer trajectory (also explained above). Similarly other quantities, namely, projections of $\Delta\mathbf{R}(t)$, tagged chain fragment-averaged density, and different entropy estimates are averaged over *t* in Figures 3 *b*, 6 *a*, 7 *a*, *b*, 8 *a*–*c* and 9. For medium length chains (C_{44}) and long chains (C_{96} and C_{100}), increased correlation is obtained between the fastest c.m. motion and the stretching of the chain, while shorter chains (C_{16} and C_{30}) being stiffer due to its small size has more propensity to be in extended state (red region in top left corner of Figure 2 *a*). Hence the representative results are shown for C_{100} in this study. As shown in Figure 3 *a*, fastest c.m. motion of polymer 10 occurs at steps-axis values in the range 2100–2300, which is increasingly correlated with large tagged chain extension values (averaged over *t*) at the same range of steps-axis values. Similarly, projections (averaged over fixed time interval *t*) of c.m. displacement along and perpendicular to the end-to-end and squared end-to-end distance values (averaged over *t*) are compared for the entire trajectory of the molecule in Figure 3 *b*. The comparison of these results in Figure 3 *b* in the steps-axis (values) range 2100–2300,

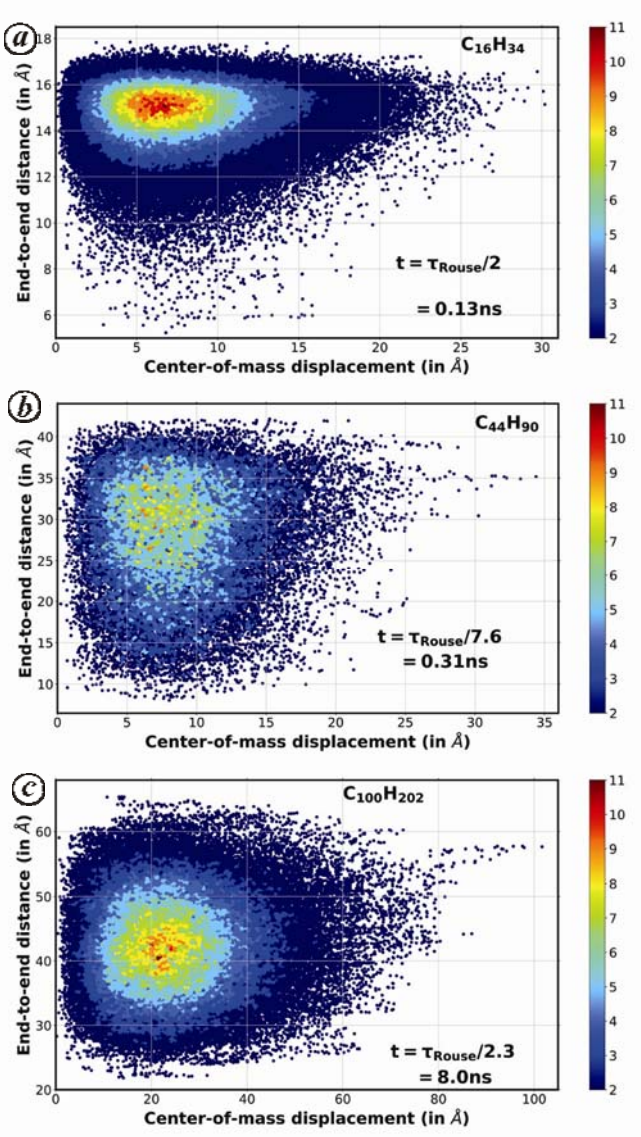

Figure 2. Contour plots of the normalized distribution of the correlation between the c.m. mean displacement and the root mean-square chain end-to-end distance at fixed time intervals $t < \tau_{Rouse}$ for (***a***) $C_{16}H_{34}$ at $t = \tau_{Rouse}/2 = 0.13$ ns, (***b***) $C_{44}H_{90}$ at $t = \tau_{Rouse}/7.6 = 0.31$ ns, and (***c***) $C_{100}H_{202}$ at $t = \tau_{Rouse}/2.3 = 8.0$ ns.

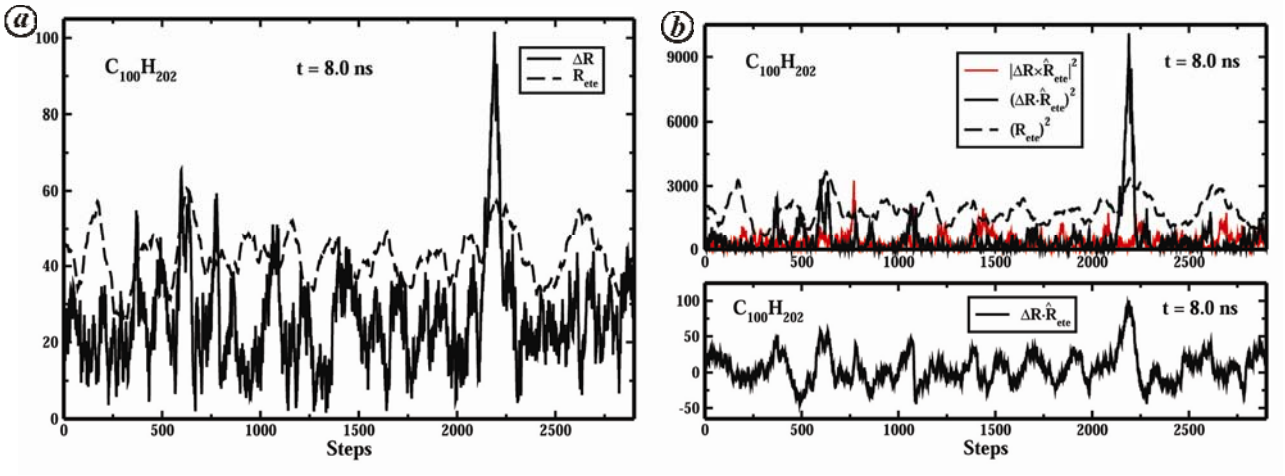

Figure 3. Correlation between extension R_{ete} and c.m. displacement ΔR, and its parallel/perpendicular component along the direction of $\mathbf{R}_{ete}$ in (***a***) and (***b***) respectively, for polymer 10 of C_{100} at time interval t = 8.0 ns.

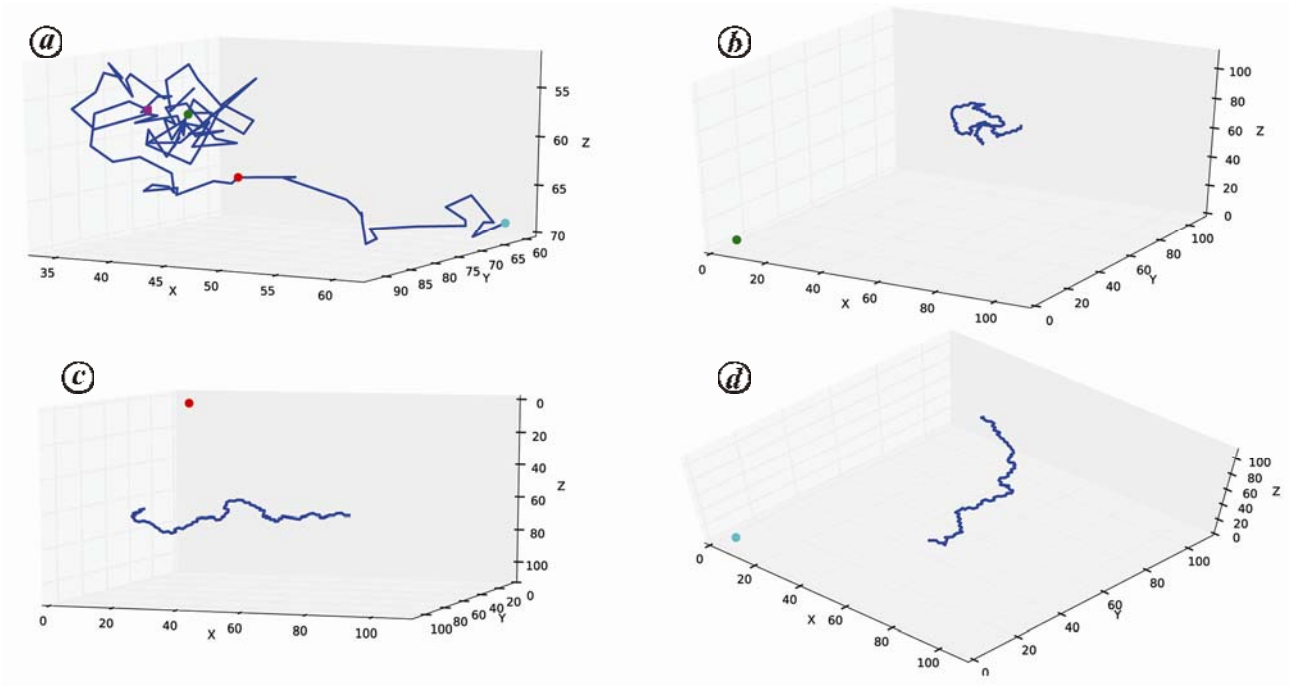

Figure 4. Molecule 11 of $C_{96}H_{194}$ PE melt: (***a***) c.m. trajectory and (***b–d***) snapshots at times marked by filled colored circles in (***a***). ●: coiled, ●: stretched, ●: reverse to coiled–conformations of the chain, and ■: onset of stretched conformations. Colored filled symbols in subfigures (***a–d***) correspond to the following real times: ● at 3.5 ns, ■ at 4.0 ns, ● at 4.4 ns, and ● at 4.875 ns.

shows that the fastest and the most part of the c.m. motion for C_{100} is along (both positive and negative) direction of the end-to-end distance; the same is true for other PE melt systems (not shown).

Molecular mechanism

The mechanism of fast dynamics is ascertained by following the c.m. motion of the molecule which exhibits the maximum heterogeneity in dynamics at a fixed time interval t. Polymer 11 of $C_{96}H_{194}$ was found to exhibit maximum heterogeneity in dynamics (as explained in previous section) at fixed time interval t = 1.85 ns. A 2.4 ns portion of the c.m. trajectory (where the fast dynamics is obtained) for polymer 11 of $C_{96}H_{194}$ is shown representatively in Figure 4 *a*, where coloured filled symbols label different (real) times along the trajectory. The snapshots of polymer configurations at times corresponding to coloured circles (in Figure 4 *a*) are shown in Figure 4 *b–d*. Early caged dynamics (●), where the polymer is sufficiently coiled (Figure 4 *b*) is followed by fast long-range unidirectional c.m. motion (●), that are correlated with the appearance of intramolecular polymer configurations having a high percentage of trans (stretched)

conformations (Figure 4 *c*), and subsequent recoiling (Figure 4 *d*) when c.m. slows down and performs short-range motion (●). ■ denotes a time after 1.5 ns of the trajectory shown in Figure 4 *a* that marks approximately the onset of relatively stretched configurations when the molecule unfolds to perform fast motion. The real time picture of this c.m. motion and corresponding polymer configurations (in the form of a movie of length 3.125 ns in real time as in simulations), exhibiting all the features as discussed for Figure 4, is in the supplement[21]. The time stamp in the movie[21] is of real time trajectory as it occurs in the simulation data. The correlation between stretched configurations and fast c.m. motion can be explicitly seen in the movie[21] between times 4.2 ns to 5.0 ns. Coloured filled symbols in Figure 4 *a–d* correspond to the following real times: ● at 3.5 ns, ■ at 4.0 ns, ● at 4.4 ns, and ● at 4.875 ns.

The analysis of c.m. trajectories (Figure 4 and the movie[21]) shows that a tagged polymer undergoes transient periods of small-amplitude motion followed by periods of large-amplitude displacements. During a short-time interval some molecules undergo local motion, while others undergo fast unidirectional diffusion[22]. Although the molecules are always partitioned between mobile and less mobile sub-populations, the identities of molecules assigned to either group change in time, and for $t > \tau_{\text{Rouse}}$, the system behaves ergodically[22]. These features are in accord with the mechanisms of heterogeneous dynamics observed in undercooled 'fragile' glass-forming liquids[6,7]. There are also similar reports of heterogeneous dynamics in supercooled polymer melts, polymer glass and polymer melts near glass transition[1–4]. Since our fragile systems are not undercooled (obvious from the T and density values calculated from Table 1), we argue that the presence of dynamical heterogeneities is due to the competition between chain connectivity and intermolecular excluded-volume interactions. This induces frustration and slowing down of global dynamics even far from the glass transition. The competition between these two effects is unique to polymer melts and concentrated solutions, and is the physical origin of the correlation hole in the structure of polymer fluids[20,23].

Two kinds of c.m. motion are predominantly observed: (i) the trivial c.m. fluctuation about a point and then recoil (caged dynamics), and (ii) the distinct switch from slow to fast dynamics; shown schematically in Figure 5, where each chain configuration (along with the c.m. shown) is a snapshot of the chain trajectory. The non-trivial second kind of motion, is further investigated, believed to be induced by the density fluctuations characteristic of the frustrated systems like undercooled fluids, and as argued earlier polymer melts represent one such system. As shown in the cartoon in Figure 5 (which is not to scale), transient low and high density regions in the melt create short lived interfaces. When a polymer end from the high density region at random happens to cross such an interface, it gets pulled by a force (shown by arrows in Figure 5) caused by this density gradient along the interface, which subsequently causes density gradient along the chain itself, resulting in simultaneous stretching of the chain and thus the whole polymer eventually gets pulled out of the high density region followed by recoiling. This reminds us of the experiments by Craighead and coworkers[24,25] and more recently by Yeh *et al.*[26], where they show that single DNA molecules in nanofluidic devices at the interface of regions containing different configurational entropies relax by *confinement induced entropy recoil mechanism*. We actually show that these density fluctuations indeed cause the switch from slow to fast dynamics in tagged polymers in melts, and further show that this switch is primarily entropy driven.

Correlation between density fluctuations and transition from slow to fast dynamics and vice-versa

The correlation between local density fluctuations about the tagged chain (the polymer chain having maximum heterogeneity in its dynamics) and its rapid switch from slow to fast dynamics, is studied. The number of monomers $n_a^k(b)$ in a spherical volume (of radius b) centered at monomer a of the tagged chain in simulation step k is calculated as

$$n_a^k(b) = 4\pi \int_0^b r^2 G_a(r,0)\mathrm{d}r. \tag{1}$$

Here $G_a(r, 0)$ is the static monomer van Hove function of the monomer a at step k. b is chosen such that it represents adequately the density fluctuations responsible for transition in the dynamics of the tagged chain. Hence the required local density about monomer a is $n_a^k(b)/V$,

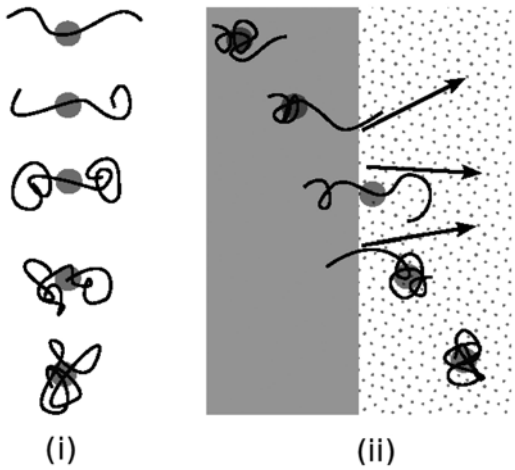

Figure 5. Schematic of two kinds of motion: (i) c.m. fluctuation and (ii) confinement induced entropy recoil mechanism. Packed circles and scattered dots resemble high and low density regions respectively. Solid filled circles represent c.m. of the chain configurations.

where $V = 4/3\pi b^3$. Since V is constant for a particular PE melt system, density fluctuations can be treated as monomer number fluctuations in volume V, and this is done consistently in the paper.

For a better representation, these calculated densities are averaged over m monomers, constituting each N/m fragments of the tagged chain, such that we have more compact fragment-wise densities of the chain, as shown representatively in Figures 6 and 7. For comparison of local densities with fast diffusion, these calculated fragment-wise densities are further averaged over time interval t as done for the calculations in Figure 3 *a*, and hence the x-axes are the same as in Figure 3 *a*. Invariably all the PE systems in Table 1 show correlation between density fluctuations about the tagged chain and fast c.m. dynamics of the fragments, results of which are shown representatively for long chain melts–polymer 10 of $C_{100}H_{202}$–and for short chain melts–polymer 20 of $C_{16}H_{34}$–in Figures 6 and 7 respectively. The tagged polymer in Figure 6 is divided into 5 fragments comprising 20 monomers each, and the results are shown in the time window of fastest dynamics, for a fixed t. Figure 6 *a* shows the results from average fragment-wise density calculations, where curve labelled (1–20) represents averaged local density about one chain end fragment, comprising first 20 monomers from one end of the tagged polymer 10 (head fragment say, in units of number of both intra and inter monomers) and the average is done over both time interval t and the comprising 20 monomers of the fragment (eq. (1)). Similarly the curve labelled (21–40), represents result as explained from the next 20 monomers following the head fragment and so on, and the curve labelled (81–100) represents explained local density results from last 20 monomers (tail fragment) at the other end of polymer 10. Similar fragment-averaging calculations are done in the rest of the paper (for Figures 6–9). Figure 6 *b* shows the c.m. dynamics of the fragments averaged over t. In Figure 6 *a*, a drop in density is first found around the chain end (tail fragment) at steps-axis values (2080–2120), which propagates till the head of the chain in time at steps-axis values (2160–2200), while parts of the chain from around middle fragment till two fragments before the tail fragment tend to remain at the high density region all through the process. Thus a gradient in density (Figure 6 *a*) exists along the chain at all times (at all steps-axis values), which gets more pronounced at steps-axis values (2080–2120). This steep density gradient along the tagged polymer and initial density drop (Figure 6 *a*) around the tail fragment at steps-axis values (2100–2105) drives the rapid switch to fast dynamics of polymer 10, with the tail performing

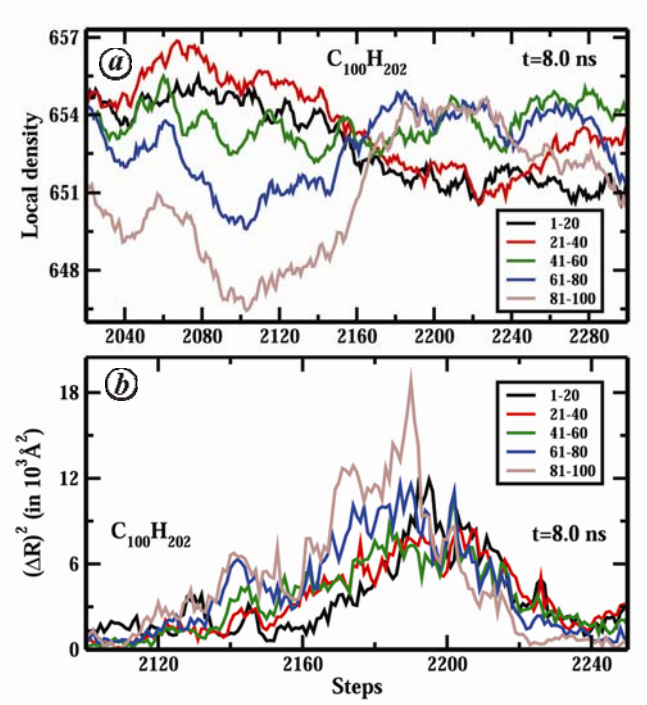

Figure 6. Average (fragment-wise) densities (in number of both intra and inter monomers) in spherical volume V (radius $b = 16.9$ Å) correlated with fragment-wise c.m. mean square displacements for 5 fragments of polymer number 10 of C_{100} melt, sampled at fixed time interval $t = 8.0$ ns. ***a***, Average fragment-wise densities; ***b***, Fragment-wise c.m. mean square displacements.

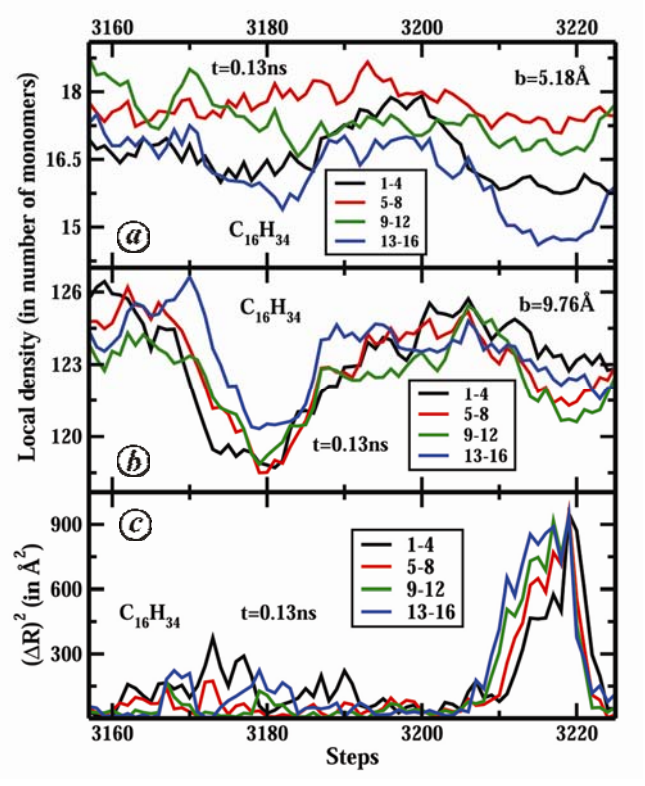

Figure 7. Average (fragment-wise) densities (in number of both intra and inter monomers) in spherical volume V correlated with fragment-wise c.m. mean square displacements for 4 fragments of polymer number 20 of C_{16} melt, sampled at $t = 0.13$ ns: (***a***) and (***b***) are densities at $b = 5.18$ Å and $b = 9.76$ Å respectively; (***c***) Fragment-wise c.m. mean square displacements.

first the fast dynamics (at steps-axis values [2160–2200]) and subsequently, pulling the rest of the chain with it by steps-axis value of 2220 as shown in Figure 6 *b*. The head fragment exhibits fast dynamics at the end of the process (at steps-axis values [2180–2220] in Figure 6 *b*). A time-lag between the density drop and the commencement of fast dynamics (from slower motion) of the chain fragments is well evident from Figure 6, with the latter event following the former; is explained by the mechanism suggested in Figure 5 (as also explained above). Thus we see parts of the chain starting from tail to head consecutively switching from slow to fast motion in the same manner as the density drop propagation along the chain, further supporting the fact that indeed density fluctuations play an important role in this rapid switch from slow to fast motion of the tagged molecule. Also it is observed that the chain is stretched to the maximum extent in the selected time window when all the fragments perform fastest dynamics (Figure 3 *b*). The same features discussed in Figure 6 *a* and *b* for C_{100} hold true for C_{96} and shown in Figure 8 *c* and *d*.

The corresponding results for melts of low molecular weight polymers are shown representatively for polymer 20 of $C_{16}H_{34}$ at fixed time interval $t = 0.13$ ns (as for Figure 2 *a*) in Figure 7 *a*–*c*, where *x*-axes are steps-axis (as defined earlier), with 0.01 ns/step (t comprises of 13 intervening steps). The tagged polymer 20 is divided into 4 fragments, each containing 4 monomers, where data from each fragment is labelled similarly as explained for Figure 6. These chain fragments (in other words the whole chain), on the contrary, perform fast dynamics almost at the same times as shown in Figure 7 *c*. This feature is attributed to the fact that short chains owing to its small size behave like particles in liquids with mass concentrated at c.m., at medium to long length scales ($\gtrapprox$ 2nd coordination shell, 9.76 Å). Hence at these length scales, individual fragments almost have similar monomer densities in volume V centered about it, at any particular instant as shown in Figure 7 *b*, unlike tagged chain fragments in long chain melts (Figure 6 *a*). Nevertheless,

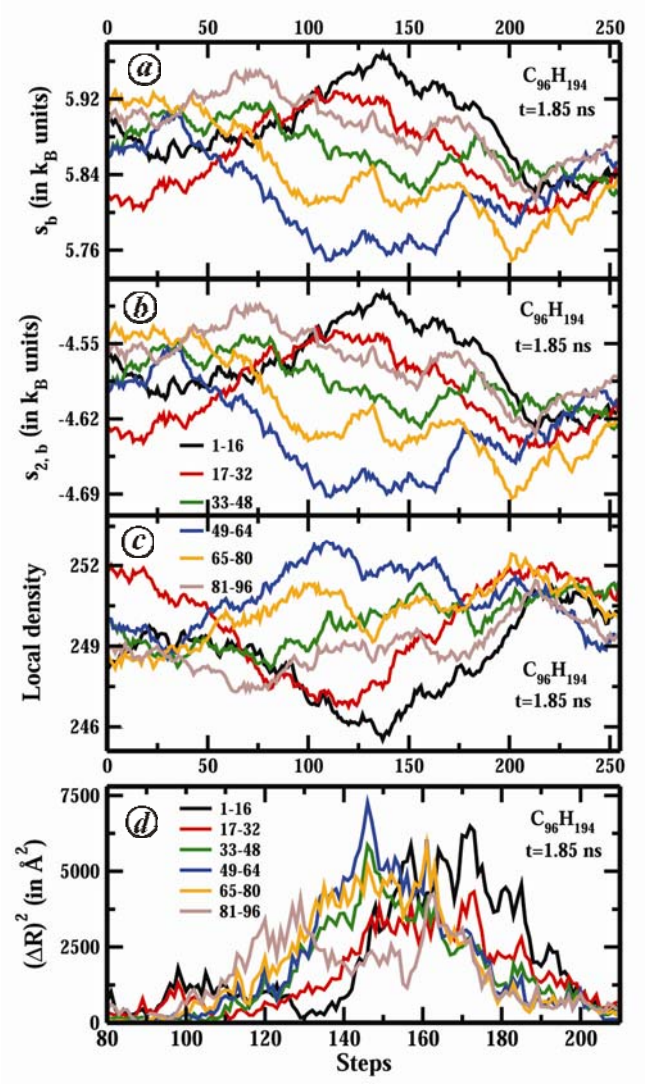

Figure 8. Average (fragment-wise) entropies s_b and $s_{2,b}$ calculated from eqs (7) and (8) and as explained in the text in a spherical volume V (radius $b = 12.22$ Å), correlated with local densities in V, for 6 fragments of polymer 11 of $C_{96}H_{194}$ melt, sampled at fixed time interval $t = 1.85$ ns: (***a***) s_b, (***b***) $s_{2,b}$, (***c***) average fragment-wise densities (in number of both intra and inter monomers) and (***d***) c.m. mean square displacement of the fragments.

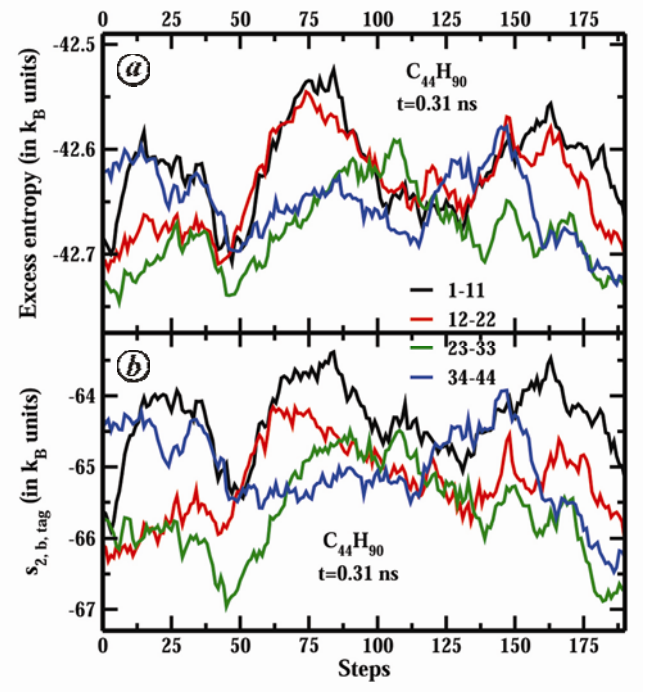

Figure 9. Comparison of average (fragment-wise) excess entropy estimates in a spherical volume V (radius $b = 12.22$ Å) from approximate method for 4 fragments of polymer number 11 of $C_{44}H_{90}$ melt, sampled at fixed time interval $t = 0.31$ ns, (***a***): Excess entropy estimates from eq. (12) and as explained in the text; (***b***): pair contribution to excess entropy $s_{2,tag}$ using eq. (7) but with $g(r)$ being of tagged chain, and also explained in the text.

drop in density in chain fragments is observed at steps-axis values (3170–3190) which subjects the whole chain to fast dynamics (Figure 7 *b* and *c*) after a time lag at steps-axis values (3210–3222). But at shorter length scales ($b \cong 5.18$ Å), the fragments show differential packing (Figure 7 *a*) and are more mobile (exhibit fast dynamics) in low density regions (see Figure 7 *a* and *c*) at steps-axis values in the ranges (3170–3190) and (3210–3222); this particular feature is almost absent for long chains (C_{100} and C_{96}). The features of correlation between density fluctuations and fast diffusion as discussed in Figure 7 *a–c* for short chain melts hold true for C_{30} and C_{44}.

Thus in long chain melts a gradient of density is observed along the chain contour of a tagged polymer and hence different portions of the chain perform fast dynamics at different times, consistent with the schematic mechanism of Figure 5, while for short chain melts, owing to its small size almost the whole chain performs fast dynamics at similar times and explicit density gradient along chain contour is not found until at short length scales. However, consistently, a drop in density either at the chain ends (for long tagged polymer) or the whole chain (for short tagged polymer) drives the switch from slow to fast dynamics.

Entropy estimation

We attempt to connect the density fluctuations to entropy of the tagged polymer. There exist various entropy and excess entropy estimation techniques in simulations[27,28] but none addresses the problem of calculating entropy in a tagged volume of dimensions – few fractions of the simulation box – centered about monomers of a particular polymer of the melt. To calculate the entropy in a spherical volume V centered about monomer a containing $M = n_a^k + 1$ monomers in a simulation step k, we first define the potential energy $V_M^a(\mathbf{r}^M)$ considering only pair interactions as

$$V_M^a(\mathbf{r}^M) = \frac{1}{2}\sum_i^M \sum_{j\neq i}^M v_{ij}(r_{ij}). \tag{2}$$

M monomers in a local volume V can be assumed to be M interacting particles in fixed volume V and the partition function can be written as[29]

$$Q_M^a(V,T) = \frac{1}{M!}\left(\frac{V}{\Lambda^3}\right)^M \frac{Z_M^a(V,T)}{V^M}, \tag{3}$$

where $\Lambda = h/\sqrt{2\pi m k_B T}$. Taking $\beta = 1/(k_B T)$, $Z_M^a(V,T)$ can be written as

$$Z_M^a(V,T) = \int \mathrm{d}\mathbf{r}^M \exp[-\beta V_M^a(\mathbf{r}^M)]$$

$$= \int \mathrm{d}\mathbf{r}_1 \ldots \mathrm{d}\mathbf{r}_N \exp\left[-\frac{\beta}{2}\sum_i^M \sum_{j\neq i}^M v_{ij}(r_{ij})\right]. \tag{4}$$

The integral in eq. (4) is possible if there is a decoupling of monomer coordinates in the integrand, but terms with v_{ij} restrict it. Instead partition function Z is written alternatively as sum over configurations with probability of each configuration calculated resulting in a solution for entropy in terms of n-particle distribution functions expressed as an intensive quantity, which is ensemble independent and is given as

$$s = \frac{S}{Mk_B} = s_{id} + \sum_{n=2}^{\infty} s_n, \tag{5}$$

where s_n is the entropy contribution due to n-particle spatial correlations and s_{id} is the ideal part representing total entropy per particle of ideal gas (in V). Assuming only pair interactions between monomers, and keeping terms until $n = 2$, eq. (5) reduces to

$$s = s_{id} + s_2 = \frac{3}{2} - \ln \rho\Lambda^3 - \frac{1}{M}\ln M! + \ln M$$

$$-2\pi\rho\int_0^{\infty}\{g(r)\ln g(r) - [g(r)-1]\}r^2\mathrm{d}r, \tag{6}$$

with s_2 being

$$s_2 = -2\pi\rho\int_0^{\infty}\{g(r)\ln g(r) - [g(r)-1]\}r^2\mathrm{d}r, \tag{7}$$

where $g(r)$ is the monomer pair distribution function and ρ is the density of monomers. Equations (5) and (6) were derived to calculate entropy for the bulk, produced results comparable to other standard techniques of entropy estimation[27]. More recently these equations were used to calculate excess entropy of liquids[30,31]. Equation (6) is modified to calculate entropy in a spherical volume V (of radius b) centered about ath monomer of tagged polymer at the kth simulation step as

$$(s_a^k)_b = \frac{3}{2} - \ln \rho\Lambda^3 - \frac{1}{M}\ln M! + \ln M$$

$$-2\pi\rho\int_0^{b}\{g(r)\ln g(r) - [g(r)-1]\}r^2\mathrm{d}r, \tag{8}$$

where $g(r)$ is the monomer pair distribution function averaged over all the monomers in V and ρ is the density of monomers in V. As before s_a^k values are averaged over

the fragment-monomers and over fixed time interval t to obtain average fragment-wise entropy expressed as an intensive quantity s_b, where subscript b denotes the radius of V. Representative results for s_b using eq. (8) are summarized in Figure 8 *a–d* for $C_{96}H_{194}$, polymer 11 at fixed time interval $t = 1.85$ ns, where x-axes are steps-axis, with 0.025 ns/step (t comprises of 74 intervening steps). The tagged polymer 11 is divided into six fragments, comprising of 16 monomers each, where data from each fragment is labelled similarly as explained for Figure 6. The s_b estimates in Figure 8 *a* have almost one-to-one mapping with the averaged fragment-wise local density values (radius $b = 12.22$ Å) in Figure 8 *c*, a peak in one corresponds to trough in the other at any step, explicitly seen at steps-axis values (100–175), and this is expected as less dense the packing of monomers in V, more conformations are available for the monomers and higher is the entropy. The corresponding $s_{2,b}$ values are calculated similarly with an analogous expression as eq. (8), averaged over t and fragment-monomers, and shown in Figure 8 *b*. Comparison of Figure 8 *a* and *b*, over the entire steps-axis values and specifically in the range (100–175), clearly indicates that the features in the s_b estimates are due to s_2 (eq. 7), the pair correlation contribution to excess entropy, consistent with earlier findings that excess entropy could explain the dynamics in supercooled fluid[32]. As expected, and also seen from Figure 8 *a* and *b*, s_{id} is almost the same for each fragment. Figure 8 *d* shows the c.m. displacements of the fragments of polymer 11, the drop in density (Figure 8 *c*) and peak in entropy (Figure 8 *a*) appears first for the tail fragment which propagates to the entire chain at steps-axis values (50–150) with the highest local density gradient (Figure 8 *c*) about the tagged chain (at the same steps-axis values). These factors drag the whole chain into the low density (high entropy) region, starting with the tail fragment performing the fast dynamics at steps-axis values >110; following it is the next connected fragment (65–80) and so on until the head fragment is pulled out by steps-axis value ≈200 as shown in Figure 8 *d*, a mechanism very similar to the tagged chain in C_{100} melt (Figure 6). Thus it is shown that the characteristic switch from slow to fast dynamics which is due to local density fluctuations about the chain ends, can be related to entropy.

Now, we discuss an alternate approximate solution of eq. (4) by approximating the potential term in eq. (1) with $\sum_{l\neq a}^{M} v_{la}(r_{la})$. This approximation implies that only pair interactions of monomer a with other monomers are considered in V, and therefore induces decoupling of the variables in eq. (4), and Z_M^a reduces to

$$Z_M^a(V,T) = V\left[\int \mathrm{d}\mathbf{r}\,\Psi_{a-1\,a}(r)\right]^2 \times\left[\int \mathrm{d}\mathbf{r}\,\Psi_{a-2\,a}(r)\right]^2 \times\left[\int \mathrm{d}\mathbf{r}\,\Psi_{a-3\,a}(r)\right]^2 \times\left[\int \mathrm{d}\mathbf{r}\,\mathrm{e}^{-\beta v_{LJ}(r)}\right]^{M-7}, \quad (9)$$

where $\Psi_{la}(\mathbf{r}_{la})$ (with $|l-a|<4$) are the intramolecular pair distribution functions, and v_{LJ} is the Lennard Jones potential. The stretch ($v_{a\pm1,a}$), bend ($v_{a\pm2,a}$) and torsion ($v_{a\pm3,a}$) potentials are written in terms of the intramolecular pair distributions and all other pair interactions are written as v_{LJ}, which are consistent with the force fields used in the simulations[17–19]. In eq. (3), $Z_M^a(V,T)/V^M$ is the excess part of the partition function, and hence excess Helmholtz free energy $A_M^{a(ex)}(V,T)$ is given as

$$\beta A_M^{a(ex)}(V,T) = -\ln\frac{Z_m^a(V,T)}{V^M} = -2\ln\left[\frac{1}{V}\int \mathrm{d}\mathbf{r}\,\Psi_{a-1\,a}(r)\right] - 2\ln\left[\frac{1}{V}\int \mathrm{d}\mathbf{r}\,\Psi_{a-2\,a}(r)\right] - 2\ln\left[\frac{1}{V}\int \mathrm{d}\mathbf{r}\,\Psi_{a-3\,a}(r)\right] - (M-7)\ln\left[\frac{1}{V}\int \mathrm{d}\mathbf{r}\,\mathrm{e}^{-\beta v_{LJ}(r)}\right], \quad (10)$$

and excess internal energy $U_M^{a(ex)}(V,T)$ can be written as

$$\beta U_M^{a(ex)}(V,T) = -\beta\frac{\partial}{\partial\beta}\ln\left[\frac{Z_M^a(V,T)}{V^M}\right] = -2\frac{\int \mathrm{d}\mathbf{r}\,\Psi_{a-1\,a}(r)\ln[\Psi_{a-1\,a}(r)]}{\int \mathrm{d}\mathbf{r}\,\Psi_{a-1\,a}(r)} - 2\frac{\int \mathrm{d}\mathbf{r}\,\Psi_{a-2\,a}(r)\ln[\Psi_{a-2\,a}(r)]}{\int \mathrm{d}\mathbf{r}\,\Psi_{a-2\,a}(r)} - 2\frac{\int \mathrm{d}\mathbf{r}\,\Psi_{a-3\,a}(r)\ln[\Psi_{a-3\,a}(r)]}{\int \mathrm{d}\mathbf{r}\,\Psi_{a-3\,a}(r)} + (M-7)\frac{\int \mathrm{d}\mathbf{r}\,\beta v_{LJ}(r)\mathrm{e}^{-\beta v_{LJ}(r)}}{\int \mathrm{d}\mathbf{r}\,\mathrm{e}^{-\beta v_{LJ}(r)}}. \quad (11)$$

Therefore, excess entropy $S_M^{a(ex)}(V,T)$ in a spherical volume centered about monomer a is given as

$$S_M^{a(ex)}(V,T)/k_B = -\beta A_M^{a(ex)}(V,T) + \beta U_M^{a(ex)}(V,T). \quad (12)$$

It is to be noted here that if calculations are done as above by taking $Q_M^a(V,T)$ instead of Z, the s_{id} as in eq. (6) is exactly reproduced, but then excess part will differ as integral in eq. (4) cannot be done directly. Substituting eqs (10) and (11) in eq. (12) excess entropy is calculated, and further averaged over fragment-monomers and over t, the representative results are shown in Figure 9 *a* for polymer 11 of C_{44} melt at fixed time interval $t = 0.31$ ns

(as for Figure 2 *b*), where *x*-axes are steps-axis, with 0.01 ns/step (*t* comprises of 31 intervening steps). The tagged polymer 11 is divided into four fragments, each containing 11 monomers, where data from each fragment is labelled similarly as explained for Figure 6. A comparison of this (approximate) method (in Figure 9 *a*) is done with another approximate calculation for s_2 where we substitute monomer pair distribution of the tagged polymer only (instead of average pair distribution of monomers in *V*, as done for Figure 8 *b*, in eq. (7) and let this quantity after averaging over *t* and fragment-monomers be denoted as $s_{2,b,\mathrm{tag}}$, and the results are shown in Figure 9 *b*. There is one-to-one mapping between features of Figure 9 *a* and *b*, almost a peak corresponds to a peak (see in steps-axis values ranges (25–100) and (125–175)), but the entropy values differ as the approximate methods differ with approximations made at different levels.

The results in Figures 8 and 9 are representative of all the polyethylene systems studies in Table 1. The small variations in individual fragment entropies as a function of time in Figures 8 *a*, *b* and 9 *a*, *b* can be explained from the fact that these values are for small volumes (few fractions of the simulation box dimensions) about the tagged polymer, and are first attempts to measure entropy in a tagged volume. Nevertheless, our study provides significant scope for further improvement on the entropy estimation methods in local volumes. To conclude this section, we could connect local density fluctuations about a tagged polymer to local entropy and consequently show that heterogeneous dynamics well above the glass transition temperature can be related to entropy.

Conclusion

To summarize, a microscopic analysis of united atom simulation data (obtained from other research groups[17–19]) is performed for unentangled polymer melts with focus on the heterogeneous dynamics. We explicitly found that the distribution of both monomer and c.m. displacements are non-Gaussian for times shorter than Rouse relaxation time due to heterogeneities in dynamics, and explored the dynamics of the tagged molecule exhibiting maximum heterogeneity. Based on the findings of the analysis of simulation data, a molecular mechanism for heterogeneous dynamics is proposed. The mechanism is based on density fluctuations, which are further related to entropy fluctuations about the tagged polymer. Various methods to estimate entropy locally in a volume about the tagged chain are explored. These methods though approximate, are able to give at least initial connections of density fluctuations and local entropy fluctuations responsible for heterogeneous dynamics in polymer melts well above their glass transition temperature. We believe similar analysis for undercooled and supercooled melts will give more developed heterogeneity in dynamics and enhanced effects compared to the present analysis.

Appendix: Derivation of $G_s(\Delta r, t)$

We consider a generic case where there are *n* polymers each containing *N* monomers, thus $G_s(\Delta r, t)$ is defined as[29]

$$G_s(\Delta r,t)=\frac{1}{nN}\left\langle\sum_{i=1}^{nN}\int \mathrm{d}\mathbf{r}'\delta[\mathbf{r}'+\Delta\mathbf{r}-\mathbf{r}_i(t)]\delta[\mathbf{r}'-\mathbf{r}_i(0)]\right\rangle, \tag{A1}$$

where $\mathbf{r}_i(t)$ and $\mathbf{r}_i(0)$ are the position vectors of monomer *i* at times *t* and 0 respectively. One such term corresponding to monomer *i* in eq. (A1) in the integrand can be written to a good approximation (based on the physical interpretation of $G_s(\Delta r, t)$) as[29]

$$\begin{aligned}\langle\delta[\mathbf{r}'+\Delta\mathbf{r}-\mathbf{r}_i(t)]\delta[\mathbf{r}'-\mathbf{r}_i(0)]\rangle &= \int \mathrm{d}\mathbf{r}_i(t)\int \mathrm{d}\mathbf{r}_i(0)P_2[\mathbf{r}_i(t)\,|\,\mathbf{r}_i(0)]\\ &\times W_1[\mathbf{r}_i(0)]\delta[\mathbf{r}'+\Delta\mathbf{r}-\mathbf{r}_i(t)]\,\delta[\mathbf{r}'-\mathbf{r}_i(0)]\\ &= P_2[\mathbf{r}'+\Delta\mathbf{r}\,|\,\mathbf{r}']W_1[\mathbf{r}'],\end{aligned} \tag{A2}$$

where P_2 is the conditional probability and W_1 is the one time equilibrium distribution function; these notations are used consistently even to represent probabilities involving normal coordinates. Hence a single term of the summation in eq. (A1), which we define as $W[\Delta r]$ can also be written as

$$\int \mathrm{d}\mathbf{r}'P_2[\Delta\mathbf{r}\,|\,\mathbf{r}']W_1[\mathbf{r}']\equiv W[\Delta r]. \tag{A3}$$

To be noted from eqs (A2) and (A3), the single term above is independent of the label specific to monomer *i*, which is true for a homogenous fluid[33]. Thus the problem reduces to deriving a generic expression for $W[\Delta r]$ and we do this by solving the equation of motion of the monomer coordinate $\mathbf{r}_a^{(i)}$ given as

$$\varsigma\frac{\mathrm{d}\mathbf{r}_a^{(i)}}{\mathrm{d}t}=-\beta^{-1}\frac{\partial\Psi[\mathbf{r}^{(i)}]}{\partial\mathbf{r}_a^{(i)}}+\mathbf{f}_a. \tag{A4}$$

The above equation is solved by expanding the monomer coordinate $\mathbf{r}_a^{(i)}$ into *N* (degree of polymerization) independent normal modes $\mathbf{x}_p$ as

$$\mathbf{r}_a^{(i)}(t)=\sum_{p=0}^{N-1}Q_{ap}\mathbf{x}_p, \tag{A5}$$

hence $\Delta\mathbf{r}_a^{(i)}(t)$, can be written as

$$\Delta \mathbf{r}_a^{(i)}(t) = \mathbf{r}_a^{(i)}(t) - \mathbf{r}_a^{(i)}(0) = \sum_{p=0}^{N-1} Q_{ap}(\mathbf{x}_p(t) - \mathbf{x}_p(0))$$

$$= \sum_{p=0}^{N-1} Q_{ap} \Delta \mathbf{x}_p(t), \quad \text{(A6)}$$

where Q are the eigenvectors. The harmonic potential Ψ enables us to decouple eq. (A5) into N independent equations of motion each corresponding to a normal mode $\mathbf{x}_p$. The distribution function of the modes $\mathbf{x}_p$ can be written as

$$P_2[\Delta \mathbf{x}_p(t) \mid \mathbf{x}_p(0)] = \left[\frac{3}{2\pi\langle x_p^2\rangle[1-\exp(-2\sigma\lambda_p t)]}\right]^{3/2}$$

$$\times \exp\left[-\frac{3}{2}\frac{[\Delta \mathbf{x}_p(t) - \mathbf{x}_p(0)(\exp(-\sigma\lambda_p t)-1)]^2}{\langle x_p^2\rangle[1-\exp(-2\sigma\lambda_p t)]}\right] (p \neq 0), \quad \text{(A7)}$$

$$P_2[\Delta \mathbf{x}_0(t) \mid \mathbf{x}_0(0)] = \left[\frac{1}{4\pi Dt}\right]^{3/2} \exp\left[-\frac{\Delta x_0(t)^2}{4Dt}\right], \quad \text{(A8)}$$

$$W_1[\mathbf{x}_p(0)] = \left[\frac{3}{2\pi\langle x_p^2\rangle}\right]^{1/2} \exp\left[-\frac{3x_p(0)^2}{2\langle x_p^2\rangle}\right], \quad \text{(A9)}$$

where λ_p is the eigenvalue and $\sigma = 3/(\zeta\beta l^2)$, with l^2 being the mean square bond length. An analogous expression as eq. (A3) can be written in terms of modes

$$W[Q_{ap}\Delta x_p(t)] = \int \mathrm{d}(Q_{ap}\mathbf{x}_p(0))\, P_2[Q_{ap}\Delta \mathbf{x}_p(t) \mid Q_{ap}\mathbf{x}_p(0)]$$

$$\times\ W_1[Q_{ap}\mathbf{x}_p(0)]. \quad \text{(A10)}$$

From eqs (A7) and (A8), eq. (A10) can be written as

$$W[Q_{ap}\Delta x_p(t)] = \left[\frac{3}{4\pi Q_{ap}^2\langle x_p^2\rangle[1-\exp(-2\sigma\lambda_p t)]}\right]^{3/2}$$

$$\times \exp\left[-\frac{3Q_{ap}^2\Delta x_p(t)^2}{4Q_{ap}^2\langle x_p^2\rangle[1-\exp(-2\sigma\lambda_p t)]}\right] (p \neq 0), \quad \text{(A11)}$$

$$W[Q_{a0}\Delta x_0(t)] = \left[\frac{1}{4\pi DtQ_{ap}^2}\right]^{3/2} \exp\left[-\frac{Q_{ap}^2\Delta x_0^2}{4DtQ_{ap}^2}\right]. \quad \text{(A12)}$$

The above formulation in terms of $Q_{ap}x_p$ and $Q_{ap}\Delta x_p$ is done to derive the distribution $W[\Delta r_a^{(i)}(t)] \equiv W[\Delta r]$ by mapping the problem to the random flight problem as described in ref. (34). In the next step we obtain $3N$-dimensional Fourier transform $A_N(\rho)$ of $W[\Delta r_a^{(i)}(t)]$ as

$$A_N(\rho) = \prod_{p=1}^{N-1} \int \mathrm{d}(Q_{ap}\Delta \mathbf{x}_p(t)) W[Q_{ap}\Delta x_p(t)] \exp[i\rho \cdot Q_{ap}\mathbf{x}_p(t)]$$

$$\times \int \mathrm{d}(Q_{a0}\Delta \mathbf{x}_0(t)) W[Q_{a0}\Delta x_0(t)] \exp[i\rho \cdot Q_{ap}\mathbf{x}_p(t)]$$

$$= \exp\left[-\frac{\rho^2}{6}\left(Q_{a0}^2(6Dt) + 2\sum_{p=1}^{N-1} Q_{ap}^2\langle x_p^2\rangle(1-\exp(-2\sigma\lambda_p t))\right)\right]$$

$$= \exp\left[-\frac{\rho^2}{6}\sum_{p=0}^{N-1} Q_{ap}^2\langle x_p^2\rangle\right] = \exp\left[-\frac{\rho^2}{6}\langle((\Delta r_a^{(i)}(t))^2\rangle\right]. \quad \text{(A13)}$$

Hence from eq. (A13), $W(\Delta r_a^{(i)}(t))$ can be written as

$$W[\Delta r_a^{(i)}(t)] = \frac{1}{8\pi^3}\int_{-\infty}^{+\infty} \mathrm{d}\rho \exp[-i\rho \cdot (\Delta r_a^{(i)})] A_N(\rho)$$

$$= \left[\frac{3}{2\pi\langle(\Delta r_a^{(i)})^2\rangle}\right]^{3/2} \exp\left[-\frac{3(\Delta r_a^{(i)})^2}{2\langle(\Delta r_a^{(i)})^2\rangle}\right]. \quad \text{(A14)}$$

Thus $G_s(\Delta r, t)$ from eqs (A2, A3 and A14) can be written as

$$G_s(\Delta r, t) = \left[\frac{3}{2\pi\langle(\Delta r)^2\rangle}\right]^{3/2} \exp\left[-\frac{3(\Delta r)^2}{2\langle(\Delta r)^2\rangle}\right]. \quad \text{(A15)}$$

In the above expression $\langle(\Delta r)^2\rangle$ is input from the simulations for the fixed time interval t.

1. Aichele, M., Gebremichael, Y., Starr, F. W., Baschnagel, J. and Glotzer, S. C., Polymer-specific effects of bulk relaxation and string like correlated motion in the dynamics of a supercooled polymer melt. *J. Chem. Phys.*, 2003, **119**, 5290–5304.
2. Deschenes, L. A. and Vanden Bout, D. A., Single-molecule studies of heterogeneous dynamics in polymer melts near the glass transition. *Science*, 2001, **292**, 255–258, and references therein.
3. Pèrez-Aparicio, R. *et al.*, Dielectric spectroscopy of a stretched polymer glass: heterogeneous dynamics and plasticity. *Macromolecules*, 2016, **49**, 3889–3898.
4. Iwaoka, N. and Takano, H., Heterogeneous chain dynamics in a supercooled polymer melt: relaxation mode analysis study. *J. Phys. Soc. Jpn.*, 2014, **83**, 123801.
5. Ye, X., Zhou, Z., Nie, Y., Ma, P., Hao, T., Yang, W. and Lu, H., Comparative study on dynamical heterogeneity of ring and linear polymers. *Macromol. Theory Simul.*, 2016, **25**, 9–15.
6. Richert, R., Heterogeneous dynamics in liquids: fluctuations in space and time. *J. Phys. Condens. Matter*, 2002, **14**, R703–R738, and references therein.

7. Ediger, M. D., Spatially heterogeneous dynamics in supercooled liquids. *Annu. Rev. Phys. Chem.*, 2000, **51**, 99–128, and references therein.
8. Panja, D., Barkema, G. T. and Ball, R. C., Complex interactions with the surroundings dictate a tagged chains dynamics in unentangled polymer melts. *Macromolecules*, 2015, **48**, 1442–1453, and references therein.
9. Kremer, K. and Grest, G. S., Dynamics of entangled linear polymer melts: A molecular dynamics simulation. *J. Chem. Phys.*, 1990, **92**, 5057–5086.
10. Wittmer, J. P., Polińska, P., Meyer, H., Farago, J., Johner, A., Baschnagel, J. and Cavallo, A., Scale-free center-of-mass displacement correlations in polymer melts without topological constraints and momentum conservation: a bond-fluctuation model study. *J. Chem. Phys.*, 2011, **134**, 234901.
11. Paul, W. *et al.*, Chain motion in an unentangled polyethylene melt: a critical test of the rouse model by molecular dynamics simulations and neutron spin echo spectroscopy. *Phys. Rev. Lett.*, 1998, **80**, 2346–2349.
12. Debnath, P. and Guenza, M. G., Cooperative dynamics in polymer melts from the unentangled to the entangled regime. *Philos. Mag.*, 2008, **33–35**, 4131–4136, and references therein.
13. Ediger, M. D. and Harrowell, P., Perspective: supercooled liquids and glasses. *J. Chem. Phys.*, 2012, **137**, 080901, and references therein.
14. Berthier, L. and Biroli, G., Theoretical perspective on the glass transition and amorphous materials. *Rev. Mod. Phys.*, 2011, **83**, 587–645, and references therein.
15. Betancourt, B. A. P., Douglas, J. F. and Starr, F. W., String model for the dynamics of glass-forming liquids. *J. Chem. Phys.*, 2014, **140**, 204509, and references therein.
16. Xu, W.-S., Douglas, J. F. and Freed, K. F., Influence of pressure on glass formation in a simulated polymer melt. *Macromolecules*, 2017, **50**, 2585–2598, and references therein.
17. Mondello, M. and Grest, G. S., Viscosity calculations of *n*-alkanes by equilibrium molecular dynamics. *J. Chem. Phys.*, 1997, **106**, 9327–9336.
18. Mondello, M., Grest, G. S., III, E. B. W. and Peczak, P., Dynamics of *n*-alkanes: comparison to rouse model. *J. Chem. Phys.*, 1998, **109**, 798–805.
19. Karayiannis, N. C. and Mavrantzas, V. G., Hierarchical modeling of the dynamics of polymers with a nonlinear molecular architecture: calculation of branch point friction and chain reptation time of H-shaped polyethylene melts from long molecular dynamics simulations. *Macromolecules*, 2005, **38**, 8583–8596.
20. de Gennes, P. G., *Scaling Concepts in Polymer Physics*, Cornell University Press, Ithaca, 1979.
21. Supplementary material: Movie of UA-MD simulation trajectory of polymer 11 of $C_{96}H_{194}$ in time window of fastest dynamics.
22. These conclusions can be made from analogous analysis as Figures 1 *a*, *b*, for c.m. dynamics and can be found in ref. 12.
23. Schweizer, K. S. and Curro, J. G., Integral equation theories of the structure, thermodynamics, and phase transitions of polymer fluids. In *Advances in Chemical Physics* (eds Prigogine, I. and Rice, S. A.), John Wiley and Sons, Inc, Hoboken, NJ, USA, 1997, vol. 98, pp. 1–142.
24. Turner, S. W. P., Cabodi, M. and Craighead, H. G., Confinement-induced entropic recoil of single DNA molecules in a nanofluidic structure. *Phys. Rev. Lett.*, 2002, **88**, 128103.
25. Mannion, J., Reccius, C., Cross, J. and Craighead, H., Conformational analysis of single DNA molecules undergoing entropically induced motion in nanochannels. *Biophys. J.*, 2006, **90**, 4538–4545.
26. Yeh, J.-W., Taloni, A., Chen, Y.-L. and Chou, C.-F., Entropy-driven single molecule tug-of-war of DNA at micro-nanofluidic interfaces. *Nano Lett.*, 2012, **12**, 1597–1602.
27. Baranyai, A. and Evans, D. J., Direct entropy calculation from computer simulation of liquids. *Phys. Rev. A*, 1989, **40**, 3817–3822, and references therein.
28. Voyiatzis, E., Müller-Plathe, F. and Bohm, M. C., Excess entropy scaling for the segmental and global dynamics of polyethylene melts. *Phys. Chem. Chem. Phys.*, 2014, **16**, 24301–24311, and references therein.
29. Hansen, J. P. and McDonald, I. R., *Theory of Simple Liquids*, Academic Press, London, 2013.
30. Sharma, R., Chakraborty, S. N. and Chakravarty, C., Entropy, diffusivity, and structural order in liquids with water like anomalies. *J. Chem. Phys.*, 2006, **125**, 204501.
31. Goel, T., Patra, C. N., Mukherjee, T. and Chakravarty, C., Excess entropy scaling of transport properties of Lennard-Jones chains. *J. Chem. Phys.*, 2008, **129**, 164904.
32. Mittal, J., Errington, J. R. and Truskett, T. M., Relationship between thermodynamics and dynamics of supercooled liquids. *J. Chem. Phys.*, 2006, **125**, 076102.
33. Boon, J. P. and Yip, S., *Molecular Hydrodynamics*, Dover Publications, Inc, New York, 1991.
34. Chandrasekhar, S., Stochastic problems in physics and astronomy. *Revs. Mod. Phys.*, 1943, **15**, 1–89.

ACKNOWLEDGEMENT. We thank Anurag Singh for help with the movie in the supplement. P.D. acknowledges the support of Science and Engineering Research Board, New Delhi (SB/FT/CS-054/2013). R.B. and N.A. gratefully acknowledge financial support from the Ministry of Human Resource and Development, India and the Institute Computer Center for computational facilities. We are grateful to V. G. Mavrantzas, G. S. Grest and coworkers for sharing UA-MD simulation trajectories.

Received 13 July 2016; revised accepted 2 June 2017

doi: 10.18520/cs/v113/i10/1974-1985